Intersystem Crossing Rates in Photoexcited Rose Bengal: Solvation versus Isolation

Aron P. Veenstra, Pascal Rauthe, Joseph Czekner, Jakob Hauns, Andreas-Neil Unterreiner, and Manfred M. Kappes*

ABSTRACT: We compare the intersystem crossing rate, k_{ISC}, of Rose Bengal (RB) in an aqueous pH 12 solution with the corresponding relaxation rates of four different RB-derived anion and dianion species isolated in the gas phase: the doubly deprotonated dianion ($[RB\text{-}2H]^{2-}$), the singly deprotonated monoanion ($[RB\text{-}H]^{-}$), and the corresponding singly negatively charged sodium and cesium adducts ($[RB\text{-}2H + Na]^{-}$ and $[RB\text{-}2H + Cs]^{-}$, respectively). Each of them was probed following photoexcitation of their first singlet excited states (S_1) at or near room temperature. The solution was studied by transient absorption spectroscopy, whereas the mass-selected anions were characterized by time-resolved photoelectron spectroscopy—all with ca. 50 femtosecond temporal resolution. $[RB\text{-}H]^{-}$ shows an S_1 lifetime of ca. 80 ps; the solution ensemble, thought to consist primarily of solvated dianion chromophores, shows a similar lifetime of ca. 70 ps. By contrast, the isolated dianion, $[RB\text{-}2H]^{2-}$, has a much longer lifetime. Superimposed on S_1 decay attributable mainly to intersystem crossing, all four isolated anions also show some rapid oscillatory features of the transient photoelectron signal on a 4−5 ps timescale after excitation. Interestingly, an analogous phenomenon is also seen in the transient absorption measurements. We attribute it to a librational oscillation as the S_1 state, initially populated in the S_0 geometry, relaxes into its excited state equilibrium structure. Some implications of these observations for RB photophysics and interpretation of solution measurements are discussed—also in terms of density functional theory and time-dependent density functional theory calculations of ground and excited states.

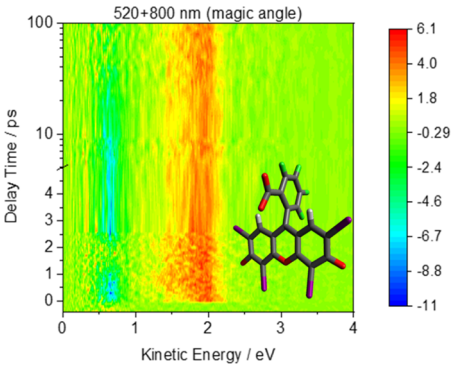

1. INTRODUCTION

Rose Bengal (RB), a fluorescein analogue, is a strongly absorbing xanthene dye that can sensitize singlet oxygen formation in solution, reflecting efficient intersystem crossing (ISC) from its initially photoexcited S_1 state to a sensitizing triplet state (triplet quantum yield, $\Phi_{ISC} > 0.9$, in phosphate buffered degassed room-temperature H_2O at a pH of 7.4).[1] Consequently, RB has many applications from staining/sensing to photodynamic cancer therapy.[2,3] As a corollary, many studies have been devoted to understanding its photophysical properties. Among these, RB solutions (in various solvents) have been extensively probed by ultrafast spectroscopy. These studies show strongly solvent dependent ISC rates ranging from quite fast in polar solution (ca. 10^{10} s^{-1} in water)[4] to more than 30 times slower in non-protic solvents (2.8×10^8 s^{-1} in acetonitrile).[5,6] This may reflect solvent mediation of spin orbit charge transfer-induced ISC processes (SOCT-ISC) as has been observed in other systems.[7,8] However, the details remain unclear because typical RB solutions can contain multiple, molecularly distinct RB-related chromophores whose relative concentrations depend on polarity and solvent pH. For example, in polar solution, the chromophore can exist in neutral, [RB], deprotonated monoanionic, $[RB\text{-}H]^{-}$, and doubly deprotonated dianionic $[RB\text{-}2H]^{2-}$ forms depending on pH.[9] Furthermore, in salt solutions, for example, of the RB disodium salt typically studied, the solvent separated or even contact ion pairs such as $[RB\text{-}2H + Na]^{-}$ may be present, leading to changed ISC rates due to modulated singlet-triplet splittings or "heavy atom effects".[10] Finally, at high enough concentrations, RB aggregates—possibly also linked by counterions—can form. Each of these distinct species has characteristic photophysical properties, and consequently, the condensed phase ISC rate measurement integrates over a range of different dynamics (again depending on the solvent and pH). To explore this, it is desirable to study the corresponding chromophores in isolation and to compare their properties with those of the solution ensemble.

Recently, first gas-phase experiments on the (static) optical properties of some of these anions have been performed. In particular, Stockett et al. have reported photoelectron and photodetachment spectra of $[RB\text{-}2H]^{2-}$ as well as (multi)

photodissociation and dispersed fluorescence spectra of isolated $[RB\text{-}H]^-$.[11] The measurements have been compared to time-dependent density functional theory (TDDFT) and higher-level calculations of the corresponding ground and electronically excited states. So far, however, there have been no measurements of the ultrashort dynamics of these species under isolated conditions. In this publication, we report measurements of the decay rate following S_1 excitation in the gas phase for (i) the singly deprotonated species, $[RB\text{-}H]^-$, (ii) the sodium and cesium adducts of the doubly deprotonated chromophore, $[RB\text{-}2H + Na]^-$ and $[RB\text{-}2H + Cs]^-$, respectively, and (iii) the doubly deprotonated $[RB\text{-}2H]^{2-}$ form. We compare these decay rates (likely due primarily to ISC) to condensed phase transient absorption spectroscopy (TAS) measurements in aqueous RB solution.

For the gas-phase measurements of the isolated anions, we have used time-resolved photoelectron spectroscopy (tr-PES), which allows us to probe the lifetimes of the corresponding photoexcited S_1 states by detaching them with a second photon after a set reaction delay. We find that under our conditions, isolated $[RB\text{-}2H]^{2-}$ as well as $[RB\text{-}2H + Na]^-$ and $[RB\text{-}2H + Cs]^-$ has (slow) decay rates comparable to the integral ISC rate of room-temperature RB solutions in non-polar solvents. By contrast, the gas-phase decay rate of $[RB\text{-}H]^-$ is faster, behaving much like the ensemble of RB chromophores in water. This is discussed qualitatively in terms of TDDFT calculations on the corresponding ions—and their associated S_1-T_1 energy gaps.

2. METHODS

2.1. Experimental Section. *2.1.1. Chemicals and Solution Characterization.* For the gas-phase experiments, anions were generally prepared by electrospray ionization of RB disodium salt (Aldrich) solutions in 4:1 methanol/water. To generate $[RB\text{-}2H + Cs]^-$, we used a solution of RB lactone (Aldrich) to which was added Cs_2CO_3 (Merck).

Static absorption spectra of RB disodium salt solutions in H_2O were recorded using a Cary 500 (Varian) spectrometer with a spectral resolution of 1 nm. TAS experiments were carried out at RB concentrations ranging between 50 and 200 μM. For all experiments, solution pH was set to 12 in order to maximize the abundance of solvated dianions (by adding 0.1 M NaOH to the aqueous RB solution in the necessary ratio).

2.1.2. Transient Absorption Spectroscopy. Transient absorption (TA) spectra in the UV–vis and near-infrared (NIR) spectral regions in aqueous solution at room temperature were recorded according to the setups and procedures described elsewhere.[12,13] In brief, for detection in the UV–vis range, a small portion of a Ti/sapphire laser system output (Astrella, Coherent, 800 nm, 1 kHz, 35 fs, 7.2 mJ, also used to provide excitation pulses for tr-PES measurements) was employed to pump a non-collinear optical parametric amplifier (NOPA). Excitation pulses centered at a wavelength of 490 nm with magic angle polarization and an energy of 0.4 μJ were obtained from the NOPA. Probe pulses between 350 and 750 nm were generated by irradiating a CaF_2 crystal to generate white light continuum. This white light was split into two pulses. The first overlapped with the pump pulse in the sample (Starna cuvette, suprasil quartz, optical path length of 1 mm, continuously stirred using a miniaturized magnetic bar) to monitor pump-induced changes as recorded using a charge-coupled device (CCD) camera (Linescan Series2000, 512 pixels, Si detector, Entwicklungsbüro Stresing). The other provided a reference pulse, which was detected using an additional CCD camera of the same type. After passing the sample and before reaching the camera, the white light was dispersed through a prism with an average resolution of roughly 1.5 nm.

Recording of TA spectra in the NIR spectral range was accomplished by using a CPA 2210 (Clark-MXR, 775 nm, repetition rate 1 kHz, 150 fs, 1.3 mJ, Ti/sapphire regenerative amplifier of a frequency doubled Er-Fibre oscillator).[13] The excitation wavelength was set to 548 nm (NOPA, magic angle) at an energy of 1.9 μJ per pulse. Probe pulses between 900 and 1600 nm were generated using a YAG crystal after seeding at 775 nm. Pump and probe pulses spatially and temporally overlapped in the sample (the same as that for the UV–vis TA experiments—see above), and the transient response was recorded using a CCD camera (Linescan Series2000, 512 pixels, InGaAs detector, Entwicklungsbüro Stresing).

Data were processed using a LabView program, which was written in-house. Every second pump pulse was blocked using an optical chopper (Thorlabs), resulting in ΔmOD (10^{-3} ΔOD, where OD represents the optical density, i.e., absorbance) spectra with and without excitation.

2.1.3. Time-Resolved Photoelectron Spectroscopy. tr-PES experiments were carried out using an ion beam apparatus described in detail elsewhere.[14] Briefly, it comprises a high-intensity electrospray ionization source that generates ions at typical vibrational energies near room temperature as well as a perpendicularly oriented linear time-of-flight mass spectrometer (TOFMS) coupled to a velocity map imaging (VMI) photoelectron spectrometer based on the Eppink-Parker[15] design. RB-derived anions were pulse-injected into the ion beam machine after 0.85 ms accumulation in the electrospray ionization (ESI) source. Ions were then pulse-extracted from the primary beam into the TOFMS and mass selected according to their flight time before entering the detachment region of the VMI photoelectron spectrometer (whose imaging axis is oriented perpendicular to the TOF flight tube). Particular care was taken to prevent contamination of the selected ion signals by decarboxylation fragments,[16] which show up at a lower mass-to-charge ratio but oftentimes in significantly higher intensities than that of the parent ions of interest here. In the detachment region, selected ions were then irradiated with either one or two spatially coincident and temporally correlated femtosecond laser pulses, yielding photoelectrons whose angular and kinetic energy distributions were determined. For this, emitted electrons were detected using a CCD camera mounted on a micro-channel plate electron multiplier detector equipped with a phosphor screen. Photoelectron (PE) spectra, that is, integrated photoelectron intensity versus electron kinetic energy, were obtained from the raw CCD data using the polar onion peeling algorithm developed by the Verlet group.[17] Energy calibration was carried out using single photon detachment of I^- at different wavelengths. In this study, we focused on dynamics occurring on timescales of a few picoseconds or larger, and consequently, all recorded photoelectron angular distributions were isotropic and are not discussed further below.

For PES experiments, we used a wavelength tunable TOPAS Prime (Light Conversion) optical parametric amplifier (OPA) pumped by the 800 nm output of a Coherent Astrella femtosecond laser (see above). TOPAS output (490–555 nm, 100–20 μJ, 55 $\pm$ 5 fs; 310–350 nm, 15–5 μJ) intensities varied from 1.8 to 7.0 $\times$ 10^9 W/cm^2.

Time-resolved photoelectron difference spectra were acquired by recording pump + probe PE spectra and subtracting from them the corresponding reference PE spectrum obtained using just the pump laser (held at the same pulse energy as that in the pump−probe measurement). The difference spectra were then collated into a contour plot of photoelectron intensity at a given electron kinetic energy (*x*-axis) versus systematically varied pump−probe delay (*y*-axis). These contour plots were then typically reduced by integrating the photoelectron signal over characteristic electron kinetic energy (EKE) ranges to yield transients reflecting the population of specific excited states at a given delay. Generally, in tr-PES measurements, the TOPAS Prime OPA provided the pump photons, while the 800 nm output of the Astrella laser or its second harmonic (400 nm) was used for the probe step. The delay between pump and probe beams was set using a computer-controlled Newport DLS 125 delay stage, and their relative polarization was in the magic angle for all experiments. This was adjusted using a $\lambda/2$ wave-plate in the 800 or 400 nm beam lines, respectively. According to the measured instrument response function, the time resolution of the tr-PES experiments reported here was 50 ± 5 fs.

2.2. Computation. DFT calculations of the $[RB\text{-}2H]^{2-}$, $[RB\text{-}H]^{-}$, and $[RB\text{-}2H + Na]^{-}$ ground states were carried out using the TURBOMOLE, V.7.4 program package.[18] Ground-state geometries were optimized with the pbe0[19−23] functional and the def2-TZVP basis set[24] for all atoms without symmetry constraints to an energetic convergence criterion of 10^{-8}.[25−27] Vibrational frequencies have been calculated using the *aoforce* module for the ground state to check for convergence and also to identify the lowest lying hindered rotations (librations) of the molecule.[28] For each of the three anions studied computationally, the 30 lowest singlet and triplet excitations were identified by the TDDFT using the *escf* routine.[29]

Beside the calculations on the RB dianion, the monoanionic radical deriving from it by removing one electron, $[RB\text{-}2H]^{\bullet-}$, has been studied to compare the theoretical and experimental electron affinities (EA2) of the system. Furthermore, EA1 values were also similarly calculated for $[RB\text{-}H]^{-}$ and $[RB\text{-}2H + Na]^{-}$.

3. RESULTS AND DISCUSSION

3.1. Static Properties. *3.1.1. Structural Features.* Figure 1 shows the computed molecular structure of the electronic ground state of $[RB\text{-}2H]^{2-}$ at the DFT level (see above). Figure S1 shows the calculated structures of the lowest energy isomeric form of $[RB\text{-}H]^{-}$ and the corresponding isomers of $[RB\text{-}2H + Na]^{-}$ and $[RB\text{-}2H + Cs]^{-}$ for reference.

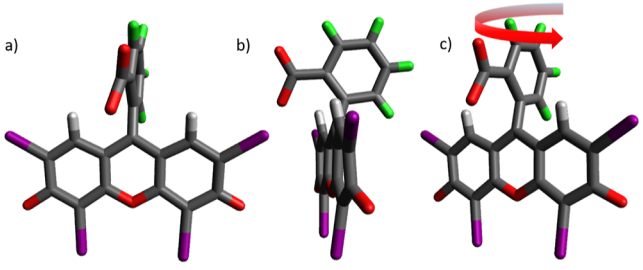

Figure 1. Front (a) and side (b) views of the ground-state structure of the doubly deprotonated RB dianion, $[RB\text{-}2H]^{2-}$ (= 4,5,6,7-tetrachloro-2′,4′,5′,7′-tetraiodofluorescein). Red corresponds to oxygen, green corresponds to chlorine, purple corresponds to iodine, and silver corresponds to hydrogen atoms. Note that the benzoic acid moiety is bound via only one C−C bond to the essentially perpendicularly oriented xanthene unit. This allows a hindered rotation (libration) motion, as schematically indicated in (c).

Given that $[RB\text{-}2H]^{2-}$ is the most abundant chromophore in pH neutral aqueous solutions according to pK_a determinations[9] (and even more so in the pH 12 solutions studied here by TAS), it is useful to begin this section with a brief overview of its main structural features. $[RB\text{-}2H]^{2-}$ consists of a near-planar xanthene framework to which is attached a benzoic acid ring oriented perpendicular to the xanthene moiety. Turning to the singly deprotonated monoanion $[RB\text{-}H]^{-}$, which is also present in a pH 7 solution as a minority species, it is interesting to note that there are two possible deprotomers. Of these, the isolated phenoxide deprotomer is calculated to be significantly more stable than the carboxylate deprotomer (by 0.35 eV, see also the Supporting Information). Therefore, we assume it to be the preferred $[RB\text{-}H]^{-}$ isomer in our experimental study—consistent also with the inferences of ref[11] Similarly, in discussing experiments on singly negatively charged counterion adducts of $[RB\text{-}2H]^{2-}$ with Cs^{+} and Na^{+}, we assume both alkali atoms to be bound at the carboxylate (see Figure S1).

One further structural point is also interesting at this juncture. Figure 1c schematically indicates a torsional motion of the benzoic acid moiety against the xanthene framework. The electronic ground state of $[RB\text{-}2H]^{2-}$ has a corresponding vibrational normal mode calculated at 20.7 cm^{-1} (1.6 ps). Interestingly, in the first excited singlet state of $[RB\text{-}2H]^{2-}$, the benzoic acid moiety is no longer oriented perpendicular to the xanthene unit but is instead slightly rotated around the common C−C bond. This is in fact a characteristic feature of all four anions studied here, which leads to torsional oscillation after vertical S_0−S_1 excitation. We show the experimental evidence for this below.

3.1.2. Electronic Absorption Properties. Figure 2 shows the electronic absorption spectrum of RB disodium salt in room-temperature water at a pH of 12 (0.05 mM). Note the appearance of a strong absorption band with a maximum at 548 nm. This corresponds primarily to the S_0−S_1 transition of the RB dianion. It is blue-shifted relative to the absorption maximum in non-protic acetonitrile by about 10 nm.[6] Stockett et al. have reported that the gas-phase (one-photon) photodetachment spectrum of $[RB\text{-}2H]^{2-}$ shows an absorption maximum at 538 ± 5 nm, whereas the multi-photon dissociation spectrum of $[RB\text{-}H]^{-}$ peaks at 545 ± 10 nm.[11]

3.1.3. Detachment Energies and Static PE Spectra. The TOPAS UV tuning range available to us did not allow the one-photon ionization of the monoanions of interest in this study. They were however detachable in our two-photon pump−probe experiments (see below). On the basis of the pump and probe wavelengths used, we can estimate the three monoanions to have electron affinities between 3.5 and 5 eV. This compares to calculated EA1 values of 3.94 eV ($[RB\text{-}H]^{-}$) and 4.02 eV for $[RB\text{-}2H + Na]^{-}$, respectively.

By contrast, $[RB\text{-}2H]^{2-}$ dianions could be readily ionized with one photon using a range of different UV−vis wavelengths (incident in the form of fs laser pulses). The resulting PE spectra are shown in Figure 3. Correspondingly, we can assign an adiabatic detachment energy (ADE) of 1.5 ± 0.1 eV to $[RB\text{-}2H]^{2-}$ (this compares with a calculated EA2 of 1.54 eV). Furthermore, we find an outer repulsive Coulomb barrier (RCB) height of 1.0 ± 0.1 eV.

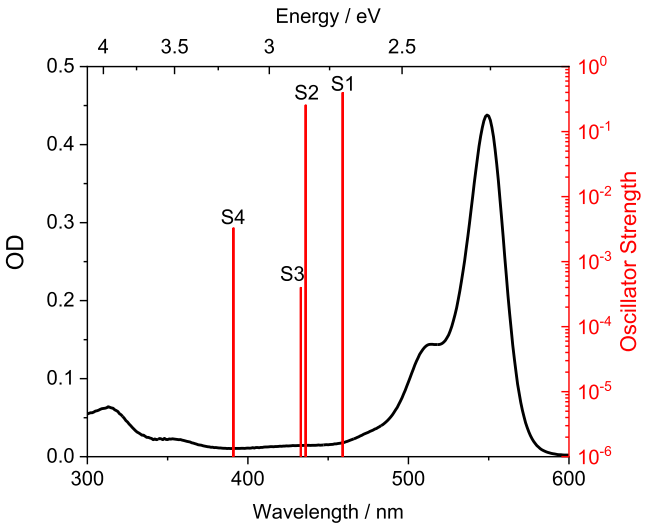

Figure 2. Comparison of the absorption spectrum of an aqueous RB solution at room temperature with vibrationless singlet electronic excitations calculated for isolated $[RB\text{-}2H]^{2-}$. Black: absorption spectrum with c = 0.05 mM (pH 12) in a 1 mm quartz cuvette. Under these conditions, the solution contains primarily the RB dianion. Red: energies and oscillator strengths of the first four singlet excitations of $[RB\text{-}2H]^{2-}$ ($S_0 \rightarrow S_n$, n = 1–4) calculated at the TDDFT level using the TURBOMOLE program package (see the Computational Results section for details).

Whereas the PE spectra of $[RB\text{-}2H]^{2-}$ recorded using varying UV detachment wavelengths show the standard EKE shifts expected for direct detachment, PE spectra recorded for the visible wavelengths show a constant EKE feature, which can be attributed to an excited state electron tunneling detachment (ESETD) process. ESETD has previously been observed by us and others for a range of other multianion systems.[30−33]

Note that Stockett et al. have reported slightly different ADE and RCB values for $[RB\text{-}2H]^{2-}$, which we attribute to some contamination of their measurement by fragmentation via CO_2 loss (a facile process for $[RB\text{-}2H]^{2-}$).

3.2. Relaxation Dynamics. *3.2.1. Transient Absorption.* A contour plot of a typical TA spectrum of a 0.1 mM solution of RB in water (at a pH of 12) after excitation at 548 nm is shown in Figure 4. This excitation wavelength was chosen because of the comparatively low response in the NIR region, whereas probing in the UV−vis spectral region was accomplished after 490 nm excitation in accordance with tr-PES (see below).

After 548 nm excitation, the spectrum shows an induced absorption peaking around 1080 nm. In line with a corresponding decrease of the first excited singlet state (see Figure S2), we interpret this response as population of a triplet state, that is, ISC, overlaid with subsequent triplet decay processes. Given the literature pK_a determination alluded to above, we assign the observed dynamics to primarily one

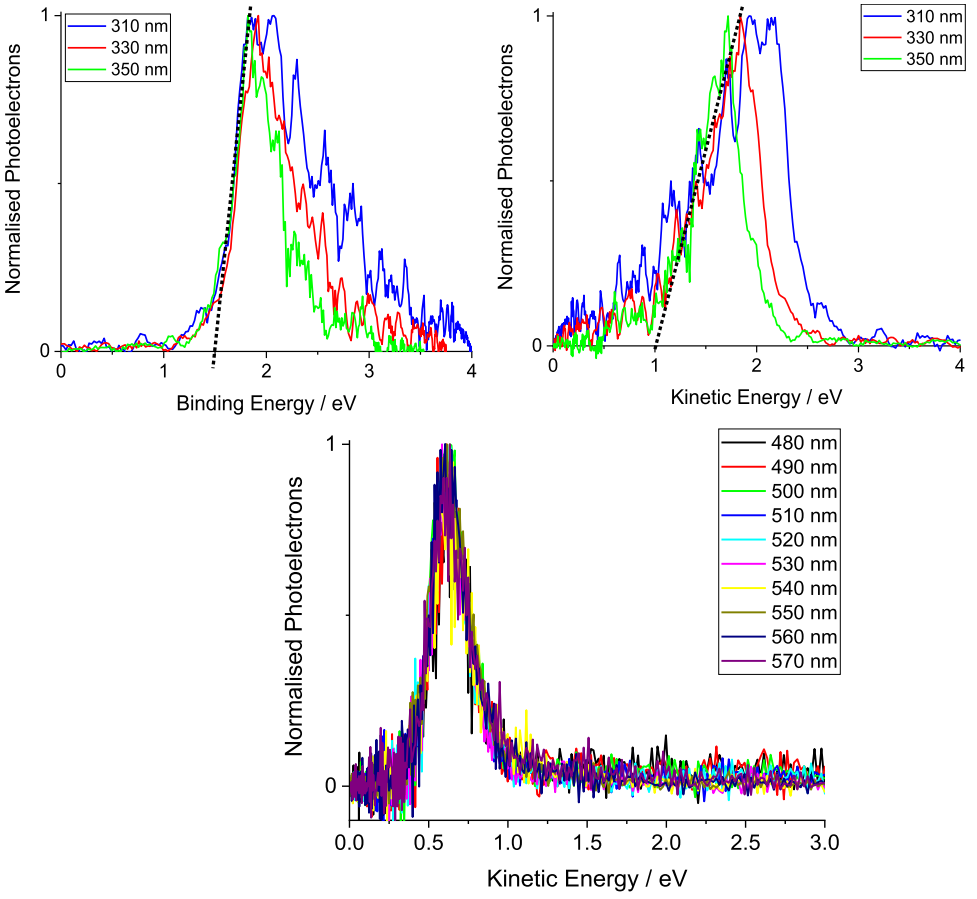

Figure 3. Top: stationary PE spectra of $[RB\text{-}2H]^{2-}$ at several wavelengths in the UV spectral range. Analysis yields ADE = 1.5 ± 0.1 eV and RCB = 1.0 ± 0.1 eV; bottom: stationary spectra in the vis spectral range. Note the detachment feature at a constant electron kinetic of 0.6 ± 0.1 eV, which we assign to an ESETD process.

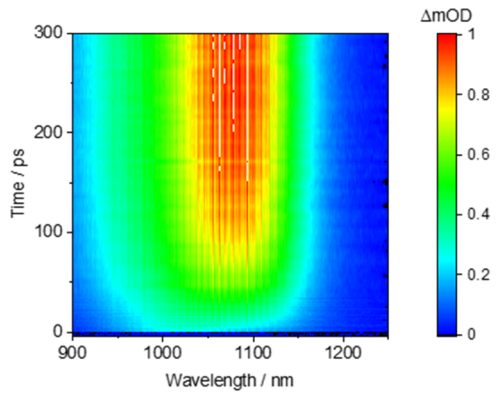

Figure 4. Contour plot of TAS in the NIR spectral region for a room temperature solution of RB in water at a pH of 12 (0.1 mM). Excitation at 548 nm with 1.9 μJ pulse energy at an OD of 0.98.

chromophore: solvated $[RB\text{-}2H]^{2-}$. Correspondingly, we assume the strong 1080 nm induced absorption to originate from the T_1 state of solvated $[RB\text{-}2H]^{2-}$ and estimate the T_2-T_1 energy difference to be ca. 1.1 eV, in line with our DFT calculations (see the Computational Results section below).

In contrast to the distinct TA NIR spectrum representing absorptive transitions from one excited (triplet) state, the UV–vis spectrum shows different contributions due to ground-state bleach around 550 nm, red-shifted stimulated emission, and excited state absorption. For direct comparison, it is helpful to extract single transient profiles from the contour plots of the UV–vis and NIR TA spectra (Figures 4 and S2a) at carefully selected wavelengths. Inspection of the TA spectra (Figure S2b) revealed a small optical window red-shifted with respect to the ground-state population around 590 nm that can be interpreted as being primarily due to stimulated emission (with a small putative contribution of the ground-state bleach) succeeded by a long-lasting absorption—later identified as triplet population. In the NIR region, the choice of an appropriate wavelength is straightforward because all transients show the same dynamics. Therefore, a peak position of the TA at 1080 nm was chosen. Both transients including exponential fit functions are shown in Figure 5. While a simple mono-exponential rise describes the NIR response very well, an exponential function with an offset for quantitative description of the response at later delay times (data points above the dashed baseline) had to be used for the 590 nm probe measurement.

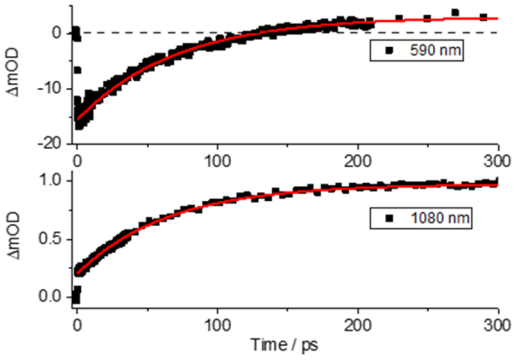

Figure 5. Single transients probed at 590 and 1080 nm after 490 and 548 nm excitation of a 0.05 mM aqueous RB solution at a pH of 12, respectively. Black squares: data points; red lines: exponential fit.

The exponential fits led to a decay time of 70 ps for a probe wavelength of 590 nm and a rise time of 65 ps for 1080 nm, respectively. Within the experimental accuracy, both values agree nicely indicating a transition from a singlet state—as identified by stimulated emission—to a triplet state with TA to higher triplet states. Another S_1-state signal was the excited-state absorption at a probe wavelength of 425 nm in the transient spectrum (Figure S2) with a lifetime of 75 ps. These time constants can be interpreted as measures of the ISC of RB in water—including the first direct triplet state observation for this molecule in the NIR region. Comparable time constants for RB in water at a pH of 9.2 of 95 ± 15 ps have been reported in an earlier work by Robinson and co-workers,[34] who analyzed fluorescence decay traces after 7 ps excitation of a frequency-doubled Nd^{3+}/glass laser (λ_{ex} = 530 nm) using subsequent streak camera detection. A comparison with TA measurements of aqueous solutions with added sodium and cesium cations as well a comparison with analogous measurements in deuterated water showed no significant differences in the lifetime (Figure S3).

Before moving on to the gas-phase measurements, we note again in passing that ISC lifetimes in RB solutions are known to change greatly depending on solvent polarity from 70 ps in water to a few nanoseconds in acetonitrile.[5,6,34,35]

3.2.2. Time-Resolved Pump–Probe Photoelectron Spectroscopy. Figure 6 shows pump–probe transients obtained for $[RB\text{-}2H]^{2-}$, $[RB\text{-}2H + Cs]^{2-}$, $[RB\text{-}2H + Na]^{-}$, and $[RB\text{-}H]^{-}$ after S_0-S_1 excitation at pump wavelengths chosen for an optimum of laser intensity and the gas-phase absorption cross-section.

As also discussed in the Methods section above, the transients were obtained for isolated electrosprayed anions (see Figure S4 for a typical mass spectrum) from contour plots of photoelectron difference spectra. The corresponding contour plots, that is, pump + probe PE spectra minus probe PE spectra versus time delay between pump and probe laser pulses, are shown in Figures S5–S7 for all four anions (in the case of $[RB\text{-}2H]^{2-}$ at two different pump wavelengths). Note that the transients shown in Figure 6 correspond to the time dependencies of S_1 populations (to the first order). In all four cases, the essentially instantaneous onset of a transient, two-color, two-photon photoelectron signal is followed by a rapid oscillatory decay to the 70–80% signal level over the 0–5 ps timescale after excitation. The expanded time scale inset in Figure 6a shows an example of this phenomenon for $[RB\text{-}2H]^{2-}$. Subsequently and on a timescale of up to 95 ps, the photoelectron signal changes much more slowly if at all—depending on the specific anion probed. We attribute the rapid initial decay to an overall reduction in the ionization cross-section as the excited-state species undergoes libration about the xanthene–benzoate bond to eventually relax into its equilibrium geometry (with a xanthene–benzoate dihedral angle of less than 90°). A similar torsional oscillation—albeit recorded with a better signal to noise—has also been reported in a pump–probe PES study of the fluorescein monoanion.[36] Given the lower quality of our data over the 0–5 ps range, which is shown in detail in Figure S8 for all four anions probed, we refrain from quantitatively analyzing it. Instead, our focus in this paper is on the slower dynamics over the 100 ps timescale, as summarized in Table 1.

Whereas the $[RB\text{-}2H]^{2-}$ and $[RB\text{-}2H + Cs]^{-}$ measurements show little further population decay from 5 ps out to the 100 ps limit probed, the S_1 populations of $[RB\text{-}2H + Na]^{-}$ and

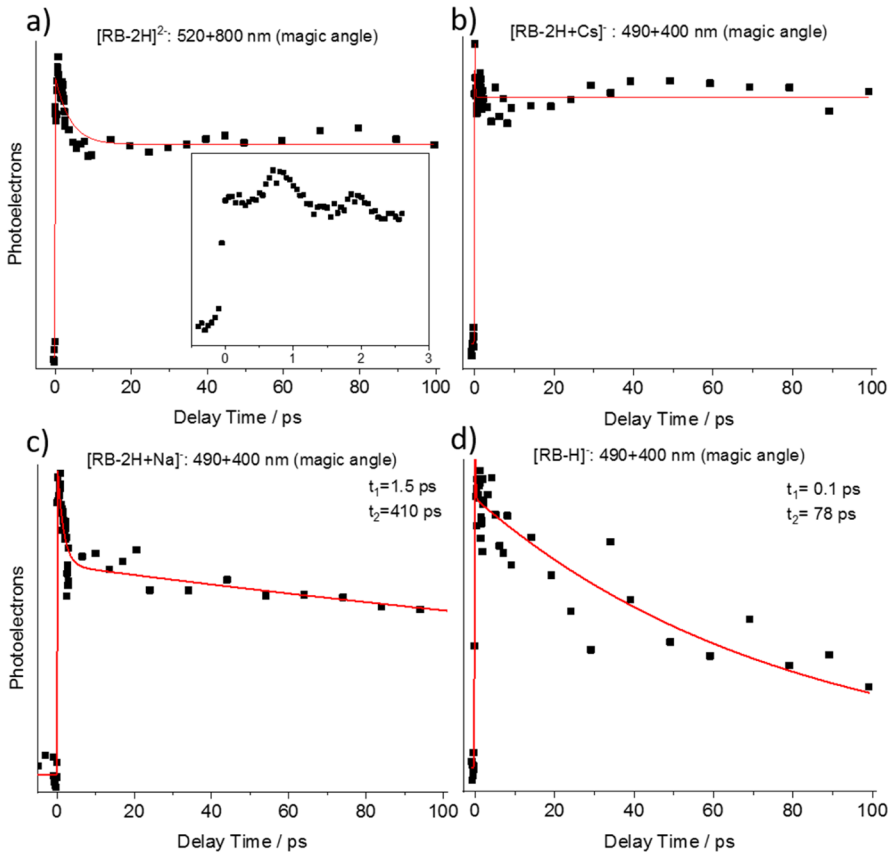

Figure 6. Integrated transients obtained from contour plots of photoelectron difference spectra (pump + probe minus pump) vs pump−probe delay. (a) $[RB\text{-}2H]^{2-}$ integrated over the 1.3−2.3 eV EKE range corresponding to the maximum in the transient PE signal (see Figure S5) Inset: Measurement with 75 fs time steps highlighting the oscillatory structure at early delay times. (b) $[RB\text{-}2H + Cs]^{-}$ (see Figure S6), (c) $[RB\text{-}2H + Na]^{-}$ (see Figure S6) and (d) $[RB\text{-}H]^{-}$ (see Figure S7) all integrated over the full EKE range to maximize the signal. See also the text for details.

Table 1. Relaxation Dynamics after S_0−S_1 Excitation[a]

ion/system	lifetime/ps
$[RB\text{-}2H]^{2-}$	≫100
$[RB\text{-}2H + Cs]^{-}$	≫100
$[RB\text{-}2H + Na]^{-}$	410
$[RB\text{-}2H + H]^{-}$	78
RB solution	75

[a]Lifetime of "slow" decay of S_1 state population attributed to ISC (superimposed rapid oscillatory decay typically completed by ca. 4 ps was not quantified due to low S/N—see the text).

$[RB\text{-}H]^{-}$ decay appreciably with lifetimes of 410 and 78 ps, respectively (see Figure 6). All four corresponding contour plots (Figures S5−S7) show no significant change in electron kinetic energy distribution over the full delay time range of 100 ps. This is a strong indicator that no further electronic state directly contributes to the transient signal. In particular, we do not observe the population onsets of triplet states presumably because they cannot be ionized with one probe laser photon at 400 nm (in contrast to the energetically higher lying S_1 states).

Concerning the tr-PES contour plots shown in the Supporting Information, three other points are also noteworthy:

(i) for $[RB\text{-}2H]^{2-}$, we also obtained data at a second pump wavelength (490 nm) with no significant change in our observations (long-lived S_1 state and no other states contributing to the contour plot), see Figure S5c,d,

(ii) the $[RB\text{-}2H]^{2-}$ contour plots show a region of negative transients due to ESETD (electron autodetachment is reduced by probe ionization), and

(iii) the tr-PES contour plot of $[RB\text{-}2H + Na]^{-}$ shows some three-photon ionization (pump + probe + probe) as an additional process.

3.3. Computational Results. S_0−S_1 transition energies in the gas phase are only known experimentally for $[RB\text{-}2H]^{2-}$ and $[RB\text{-}H]^{-}$ (from the work of Stockett et al).[11] There are no analogous measurements for $[RB\text{-}2H + Na]^{-}$ and $[RB\text{-}2H + Cs]^{-}$. Furthermore, triplet-state energies are not available from the experiment for each of the four isolated anions studied.

For this reason, we have calculated singlet- and triplet-state energies for the corresponding anions using TDDFT at the level described in the Computation section. These are shown in Table 2.

Note that predictions of electronic π−π^* excitations of rhodamine dyes using time-dependent Kohn−Sham theory, for example, TDDFT calculations of the S_0−S_1 transition energies of RB anions, as performed here, are known to suffer from the "cyanine problem" (first observed in analogous calculations of cyanine dyes). This arises from intrinsically inadequate treatment of the differential electron correlation between ground and excited states and makes predicted S_1−S_0 and S_1−T_1 gaps quantitatively unreliable (and strongly dependent on the functional).[37,38] Therefore, for comparing to our experimental data, we can only consider global trends in the predicted energies, as listed in Table 2. These show (relative to

Table 2. Energies of the Lowest Lying Calculated Singlet and Triplet Excitations of $[RB\text{-}2H]^{2-}$, $[RB\text{-}H]^{-}$, and $[RB\text{-}2H + Na]^{-}$ (Relative to Their Respective Singlet Ground States)[a]

singlets	relative energy [eV]	oscillator strength	triplets	relative energy [eV]
		$[RB\text{-}2H]^{2-}$		
S_1	2.70	0.3971	T_1	1.61
S_2	2.84	0.2560	T_2	2.64
S_3	2.86	0.0004	T_3	2.78
S_4	3.17	0.0033	T_4	2.83
		$[RB\text{-}H]^{-}$[b]		
S_1	2.54	0.1609	T_1	1.39
S_2	2.63	0.4467	T_2	2.39
S_3	2.67	0.0561	T_3	2.54
S_4	2.90	0.0064	T_4	2.64
		$[RB\text{-}2H + Na]^{-}$[b]		
S_1	2.66	0.5705	T_1	1.52
S_2	3.00	0.0231	T_2	2.52
S_3	3.23	0.0002	T_3	2.77
S_4	3.38	0.0339	T_4	2.97

[a]For excited singlet states, we also give oscillator strengths (derived using the dipole velocity formula). [b]Phenoxide isomer, that is protonated/sodiated carboxylate (see also the Supporting Information).

the corresponding dianion state energies) a reduction of S_1 and T_1 energies by 0.16 and 0.22 eV, respectively—depending on the counterion attached to the carboxylate. More detailed inferences require higher-level calculations that go beyond the scope of this study.

4. CONCLUSIONS

We have used tr-PES to study the decay dynamics of the isolated chromophores $[RB\text{-}2H]^{2-}$, $[RB\text{-}H]^{-}$, $[RB\text{-}2H + Na]^{-}$, and $[RB\text{-}2H + Cs]^{-}$ following S_1 photoexcitation and have compared their dynamic response to TA measurements carried out for an aqueous pH 12 solution of RB disodium salt at room temperature (containing primarily solvated $[RB\text{-}2H]^{2-}$). All four isolated anions show a rapid oscillatory decay of their S_1 related probe signals (to a base level of 70−80% of the initial signal) on a timescale of 0−4 ps following excitation. We attribute this to structural relaxation via a torsional oscillation of the benzyl moiety against the xanthene framework (as has been observed in a related study of the fluorescein monoanion).[36] Interestingly, preliminary TA measurements also show a similar oscillatory decay in solution (see Figure S9). Apart from improving experimental *S*/*N* ratios to allow better quantification of the corresponding rapid oscillatory decay phenomena in both gas and solution phases, dynamical simulations should be carried out in future to quantitatively understand how the (dissipative) dynamics of torsional oscillations in the corresponding S_1 states depend on the environment.

For $[RB\text{-}2H + Na]^{-}$ and in particular for $[RB\text{-}H]^{-}$, the initial oscillatory relaxation is followed by a further appreciable transient signal reduction with time constants of 410 and 78 ps, respectively. By contrast, $[RB\text{-}2H]^{2-}$ and $[RB\text{-}2H + Cs]^{-}$ do not undergo a measurable decay over the 100 ps timescale probed. From the corresponding tr-PES contour plots, we infer that we are detaching only from the respective S_1 state populations—no other excited electronic states are being directly probed in the tr-PES measurements. Consequently, for isolated $[RB\text{-}2H]^{2-}$ and $[RB\text{-}2H + Cs]^{-}$, the ISC time constants must be much longer than 100 ps. The observation of some ESETD (integrated in the detachment region of the VMI spectrometer over nanosecond timescales) in the case of photoexcited $[RB\text{-}2H]^{2-}$ suggests that in this dianion system, ISC is in fact slow enough that ESETD can become competitive. By contrast, we interpret the decay time constants of $[RB\text{-}2H + Na]^{-}$ and in particular of $[RB\text{-}H]^{-}$ (both of which cannot undergo ESETD) to indicate that they have much faster ISC rates than isolated $[RB\text{-}2H]^{2-}$ and $[RB\text{-}2H + Cs]^{-}$.

The ISC time constant of 65−75 ps determined in this study for a pH 12 aqueous solution of RB is quite similar to the S_1 lifetime of 78 ps determined for gas-phase $[RB\text{-}H]^{-}$. This is probably fortuitous as the chromophores being compared are significantly different molecularly. On one hand, we are probing an isolated monoanion probably with deprotonated phenoxide and protonated carboxylate group.[11] On the other hand, we are probing a dianion embedded in a water solvation shell in which the two negative charges mainly localized on carboxylate and phenoxide groups, respectively, interact dynamically with the water hydrogen bonding network. Remarkably though, the large almost 2 orders of magnitude spread in ISC rates of RB in solution (from polar water to non-polar acetonitrile)[6] can be matched in isolated anions simply by attaching a proton to the COO^{-} group of $[RB\text{-}2H]^{2-}$, thus going from the dianion $[RB\text{-}2H]^{2-}$, which behaves in terms of its decay rate like RB solvated in acetonitrile, to $[RB\text{-}H]^{-}$, which behaves like RB in aqueous solution at a pH of 12.

To what extent these parallels between integral ISC rates in the condensed phase and the decay rates of discrete anionic chromophores in the gas phase have a common origin remains unclear at this stage. It is however interesting to note that our (qualitative) TDDFT calculations on the isolated monoanions find that S_1-T_1 energy gaps can vary by 0.2 eV simply by substituting counterion adducts along the series $RB\text{-}2H^{2-}\cdots X^{+}$ (X = H, Na, and Cs). Thus, according to a simple energy gap picture, ISC rates should also vary correspondingly. This would surely also be a relevant issue for ionic solutions prone to contact pair formation. In addition, differential solvent stabilization of S_1 and T_1 states would be expected to strongly depend on whether the localized negative charge(s) on the RB unit are in contact with a counterion or whether on average they form a solvent separated ion pair. Finally, SOCT-induced ISC processes would clearly be influenced both by contact ion pairs and polar solvent molecules.

To sort this out in future, a combination of additional experiments [including varied solvent viscosity, systematically varied pH (in analogy to recent nitrophenol studies),[39] studies in both the condensed and gas phase at lower temperatures, probes of isolated RB anions aggregated with a defined number of water molecules, and so on) and ab initio molecular dynamics simulations together with higher-level (and more reliable) excited-state predictions is called for. In general, our study of isolated anions highlights the likelihood that molecularly distinct members of an ionic chromophore family simultaneously present in solution may show extremely different ISC dynamics. Conversely, understanding ISC in such solutions requires information about all separately contributing chromophores.

■ ASSOCIATED CONTENT

Additional measurements and calculations: DFT ground-state structures for $[RB\text{-}H]^-$ and $[RB\text{-}2H + Na]^-$; TDDFT calculations of excited singlet and triplet states for the $[RB\text{-}H]^-$ alcohol isomer; TAS contour plot and TA measurements of aqueous RB solutions; TA for aqueous RB solutions at a pH of 12 after excitation @ 530 nm; Orbitrap ESI mass spectrum of RB disodium salt solution; tr-PES contour plot and transients of $[RB\text{-}2H]^{2-}$; tr-PES contour diagrams of $[RB\text{-}2H + Cs]^-$ and $[RB\text{-}2H + Na]^-$' tr-PES contour diagram of $[RB\text{-}H]^-$; and plots of short timescale oscillations in integrated transient photoelectron signals (pump + probe minus probe) for all four RB species studied as well as one example in the solution phase as obtained from TAS (PDF)

■ AUTHOR INFORMATION

Corresponding Author

Manfred M. Kappes − *Institute of Physical Chemistry (IPC), KIT, 76128 Karlsruhe, Germany; Institute of Nanotechnology (INT) and Institute of Quantum Materials and Technology (IQMT), KIT, 76344 Eggenstein-Leopoldshafen, Germany;* orcid.org/0000-0002-1199-1730; Email: Manfred.Kappes@kit.edu

Authors

Aron P. Veenstra − *Institute of Physical Chemistry (IPC), KIT, 76128 Karlsruhe, Germany;* orcid.org/0000-0002-7658-102X

Pascal Rauthe − *Institute of Physical Chemistry (IPC), KIT, 76128 Karlsruhe, Germany*

Joseph Czekner − *Institute of Physical Chemistry (IPC), KIT, 76128 Karlsruhe, Germany;* orcid.org/0000-0002-7013-8334

Jakob Hauns − *Institute of Physical Chemistry (IPC), KIT, 76128 Karlsruhe, Germany;* orcid.org/0000-0001-7620-5035

Andreas-Neil Unterreiner − *Institute of Physical Chemistry (IPC), KIT, 76128 Karlsruhe, Germany;* orcid.org/0000-0002-1225-5460

Notes

The authors declare no competing financial interest.

■ ACKNOWLEDGMENTS

The tr-PES measurements were funded by the Deutsche Forschungsgemeinschaft (DFG) under SFB TRR 88 ("3MET"), project C6. The TA investigations in the liquid phase were part of projects in the DFG funded GRK 2039 "Molecular architecture for fluorescent cell imaging". M.K. and A.N.U. also thank DFG for funding the femtosecond laser system used in this work under INST 121384/133-1FUGG. They also thank KSOP and KIT/Land B.-W. for partial support of this research. J.C. would also like to thank the Alexander von Humboldt Foundation for the funding of a postdoctoral fellowship.

■ REFERENCES

(1) Berndt, O.; Bandt, F.; Eichwurzel, I.; Stiel, H. Picosecond Transient Absorption of Xanthene Dyes. *Acta Phys. Pol., A* **1999**, *95*, 207−220.

(2) Alexander, W. Rose Bengal: From a Wool Dye to a Cancer Therapy. *Powder Technol.* **2010**, *35*, 469.

(3) Qin, J.; Kunda, N.; Qiao, G.; Calata, J. F.; Pardiwala, K.; Prabhakar, B. S.; Maker, A. V. Colon Cancer Cell Treatment with Rose Bengal Generates a Protective Immune Response via Immunogenic Cell Death. *Cell Death Dis.* **2017**, *8*, No. e2584.

(4) Penzkofer, A.; Simmel, M.; Riedl, D. Room Temperature Phosphorescence Lifetime and Quantum Yield of Erythrosine B and Rose Bengal in Aerobic Alkaline Aqueous Solution. *J. Lumin.* **2012**, *132*, 1055−1062.

(5) Stracke, F.; Heupel, M.; Thiel, E. Singlet Molecular Oxygen Photosensitized by Rhodamine Dyes: Correlation with Photophysical Properties of the Sensitizers. *J. Photochem. Photobiol., A* **1999**, *126*, 51−58.

(6) Ludvíková, L.; Friš, P.; Heger, D.; Šebej, P.; Wirz, J.; Klán, P. Photochemistry of Rose Bengal in Water and Acetonitrile: a Comprehensive Kinetic Analysis. *Phys. Chem. Chem. Phys.* **2016**, *18*, 16266−16273.

(7) Pomarico, E.; Pospíšil, P.; Bouduban, M. E. F.; Vestfrid, J.; Gross, Z.; Záliš, S.; Chergui, M.; Vlček, A. Photophysical Heavy-Atom Effect in Iodinated Metallocorroles: Spin−Orbit Coupling and Density of States. *J. Phys. Chem. A* **2018**, *122*, 7256−7266.

(8) Cannizzo, A.; Blanco-Rodríguez, A. M.; El Nahhas, A.; Šebera, J.; Záliš, S.; Vlček, A.; Chergui, M. Femtosecond Fluorescence and Intersystem Crossing in Rhenium(I) Carbonyl−Bipyridine Complexes. *J. Am. Chem. Soc.* **2008**, *130*, 8967−8974.

(9) Batistela, V. R.; Pellosi, D. S.; de Souza, F. D.; da Costa, W. F.; de Oliveira Santin, S. M.; de Souza, V. R.; Caetano, W.; de Oliveira, H. P. M.; Scarminio, I. S.; Hioka, N. pKa Determinations of Xanthene Derivates in Aqueous Solutions by Multivariate Analysis Applied to UV−Vis Spectrophotometric Data. *Spectrochim. Acta, Part A* **2011**, *79*, 889−897.

(10) Cavanagh, M. C.; Larsen, R. E.; Schwartz, B. J. Watching Na Atoms Solvate into (Na^+,e^-) Contact Pairs: Untangling the Ultrafast Charge-Transfer-to-Solvent Dynamics of Na^- in Tetrahydrofuran (THF). *J. Phys. Chem. A* **2007**, *111*, 5144−5157.

(11) Stockett, M. H.; Kjær, C.; Daly, S.; Bieske, E. J.; Verlet, J. R.; Nielsen, S. B.; Bull, J. N. Photophysics of Isolated Rose Bengal Anions. *J. Phys. Chem. A* **2020**, *124*, 8429−8438.

(12) Schweigert, C.; Babii, O.; Afonin, S.; Schober, T.; Leier, J.; Michenfelder, N. C.; Komarov, I. V.; Ulrich, A. S.; Unterreiner, A. N. Real-Time Observation of Diarylethene-Based Photoswitches in a Cyclic Peptide Environment. *ChemPhotoChem* **2019**, *3*, 403−410.

(13) Michenfelder, N. C.; Gienger, C.; Dilanas, M.; Schnepf, A.; Unterreiner, A.-N. Photoexcitation of Ge_9^- Clusters in THF: New Insights into the Ultrafast Relaxation Dynamics and the Influence of the Cation. *Molecules* **2020**, *25*, 2639.

(14) Veenstra, A. P.; Monzel, L.; Baksi, A.; Czekner, J.; Lebedkin, S.; Schneider, E. K.; Pradeep, T.; Unterreiner, A.-N.; Kappes, M. M. Ultrafast Intersystem Crossing in Isolated $Ag_{29}(BDT)_{12}^{3-}$ Probed by Time-Resolved Pump−Probe Photoelectron Spectroscopy. *J. Phys. Chem. Lett.* **2020**, *11*, 2675−2681.

(15) Eppink, A. T. J. B.; Parker, D. H. Velocity Map Imaging of Ions and Electrons Using Electrostatic Lenses: Application in Photoelectron and Photofragment Ion Imaging of Molecular Oxygen. *Rev. Sci. Instrum.* **1997**, *68*, 3477−3484.

(16) Graul, S. T.; Squires, R. R. The Existence of Alkyl Carbanions in the Gas Phase. *J. Am. Chem. Soc.* **1988**, *110*, 607−608.

(17) Roberts, G. M.; Nixon, J. L.; Lecointre, J.; Wrede, E.; Verlet, J. R. R. Toward Real-Time Charged-Particle Image Reconstruction Using Polar Onion-Peeling. *Rev. Sci. Instrum.* **2009**, *80*, 053104.

(18) TURBOMOLE. V7.4.1 2019, a development of University of Karlsruhe and Forschungszentrum Karlsruhe GmbH, 1989-2007, TURBOMOLE GmbH, since 2007; available from http://www.turbomole.com (accessed Oct 10, 2022).

(19) Dirac, P. A. M. Quantum Mechanics of Many-Electron Systems. *Proc. R. Soc. London, Ser. A* **1929**, *123*, 714−733.
(20) Slater, J. C. A Simplification of the Hartree-Fock Method. *Phys. Rev.* **1951**, *81*, 385.
(21) Perdew, J. P.; Burke, K.; Ernzerhof, M. Generalized Gradient Approximation Made Simple. *Phys. Rev. Lett.* **1996**, *77*, 3865.
(22) Perdew, J. P.; Ernzerhof, M.; Burke, K. Rationale for Mixing Exact Exchange with Density Functional Approximations. *J. Chem. Phys.* **1996**, *105*, 9982−9985.
(23) Perdew, J. P.; Wang, Y. Accurate and Simple Analytic Representation of the Electron-Gas Correlation Energy. *Phys. Rev. B* **1992**, *45*, 13244.
(24) Weigend, F.; Ahlrichs, R. Balanced Basis Sets of Split Valence, Triple Zeta Valence and Quadruple Zeta Valence Quality for H to Rn: Design and Assessment of Accuracy. *Phys. Chem. Chem. Phys.* **2005**, *7*, 3297−3305.
(25) Häser, M.; Ahlrichs, R. Improvements on the Direct SCF Method. *J. Comput. Chem.* **1989**, *10*, 104−111.
(26) Treutler, O.; Ahlrichs, R. Efficient Molecular Numerical Integration Schemes. *J. Chem. Phys.* **1995**, *102*, 346−354.
(27) Eichkorn, K.; Weigend, F.; Treutler, O.; Ahlrichs, R. Auxiliary Basis Sets for Main Row Atoms and Transition Metals and their Use to Approximate Coulomb Potentials. *Theor. Chem. Acc.* **1997**, *97*, 119−124.
(28) Deglmann, P.; May, K.; Furche, F.; Ahlrichs, R. Nuclear Second Analytical Derivative Calculations Using Auxiliary Basis Set Expansions. *Chem. Phys. Lett.* **2004**, *384*, 103−107.
(29) Bauernschmitt, R.; Häser, M.; Treutler, O.; Ahlrichs, R. Calculation of Excitation Energies within Time-Dependent Density Functional Theory Using Auxiliary Basis Set Expansions. *Chem. Phys. Lett.* **1997**, *264*, 573−578.
(30) Dau, P. D.; Liu, H.-T.; Yang, J.-P.; Winghart, M.-O.; Wolf, T. J.; Unterreiner, A.-N.; Weis, P.; Miao, Y.-R.; Ning, C.-G.; Kappes, M. M. Resonant Tunneling through the Repulsive Coulomb Barrier of a Quadruply Charged Molecular Anion. *Phys. Rev. A* **2012**, *85*, 064503.
(31) Winghart, M.-O.; Yang, J.-P.; Kühn, M.; Unterreiner, A.-N.; Wolf, T. J.; Dau, P. D.; Liu, H.-T.; Huang, D.-L.; Klopper, W.; Wang, L.-S.; Kappes, M. M. Electron Tunneling from Electronically Excited States of Isolated Bisdisulizole-Derived Trianion Chromophores Following UV Absorption. *Phys. Chem. Chem. Phys.* **2013**, *15*, 6726−6736.
(32) Jäger, P.; Brendle, K.; Schwarz, U.; Himmelsbach, M.; Armbruster, M. K.; Fink, K.; Weis, P.; Kappes, M. M. Q and Soret Band Photoexcitation of Isolated Palladium Porphyrin Tetraanions Leads to Delayed Emission of Nonthermal Electrons over Microsecond Time Scales. *J. Phys. Chem. Lett.* **2016**, *7*, 1167−1172.
(33) Winghart, M. O.; Yang, J. P.; Vonderach, M.; Unterreiner, A. N.; Huang, D. L.; Wang, L. S.; Kruppa, S.; Riehn, C.; Kappes, M. M. Time-Resolved Photoelectron Spectroscopy of a Dinuclear Pt(II) Complex: Tunneling Autodetachment from both Singlet and Triplet Excited States of a Molecular Dianion. *J. Chem. Phys.* **2016**, *144*, 054305.
(34) Fleming, G.; Knight, A.; Morris, J.; Morrison, R.; Robinson, G. Picosecond Fluorescence Studies of Xanthene Dyes. *J. Am. Chem. Soc.* **1977**, *99*, 4306−4311.
(35) Cramer, L. E.; Spears, K. G. Hydrogen Bond Strengths from Solvent-Dependent Lifetimes of Rose Bengal Dye. *J. Am. Chem. Soc.* **1978**, *100*, 221−227.
(36) Horke, D. A.; Chatterley, A. S.; Bull, J. N.; Verlet, J. R. R. Time-Resolved Photodetachment Anisotropy: Gas-Phase Rotational and Vibrational Dynamics of the Fluorescein Anion. *J. Phys. Chem. Lett.* **2015**, *6*, 189−194.
(37) Moore, B., II; Schrader, R. L.; Kowalski, K.; Autschbach, J. Electronic π-to-π^* Excitations of Rhodamine Dyes Exhibit a Time-Dependent Kohn−Sham Theory "Cyanine Problem". *ChemistryOpen* **2017**, *6*, 385−392.
(38) Zhou, P. Why the Lowest Electronic Excitations of Rhodamines are Overestimated by Time-Dependent Density Functional Theory. *Int. J. Quantum Chem.* **2018**, *118*, No. e25780.
(39) Leier, J.; Michenfelder, N. C.; Unterreiner, A.-N.; Olzmann, M. Indications for an Intermolecular Photo-Induced Excited-State Proton Transfer of p-Nitrophenol in Water. *Mol. Phys.* **2021**, *119*, No. e1975051.